IEEE Control Systems Letters paper presented at
2023 American Control Conference (ACC)
San Diego, CA, USA. May 31 - June 2, 2023

Altitude Control of a Tethered Multi-Rotor Autogyro in 2-D Using Pitch Actuation via Differential Rotor Braking

Tasnia Noboni[1], Jonathan McConnell[2] and Tuhin Das[3]

***Abstract*— For tethered multi-rotor autogyros to be viable energy efficient unmanned aerial vehicles (UAVs), control analysis and stability investigation of autorotative flight are vital. In this paper, a simplified model-based altitude control technique is presented which is effective in the presence of both uniform and variable wind profile. A two-rotor autogyro, tethered to the ground and constrained to move in the 2D plane of the wind direction, is adopted for the study. The reduction to 2D simplifies the system and helps focus on the feasibility of altitude control and pitch modulation by exclusively using differential braking, which is a novel concept. In this arrangement, control inputs are the braking torques in each of the two rotors. The assumption is that with another two rotors in the lateral direction the roll and yaw motion of the system can be controlled when extended to 3D. The aerodynamics and tether modeling are based on Blade Element Momentum (BEM) method and catenary mechanics respectively. The characteristics of the equilibria of the tethered multi-rotor autogyro are investigated. For the aforementioned set-up, the differential rotor braking input is designed based on a proportional feedback law, and is effective in controlling the autogyro's altitude with the help of restoring effect provided by the tether tension.**

I. INTRODUCTION

Autogyro is a rotorcraft that produces lift by using unpowered rotor(s) which turn(s) by the action of relative airflow through the blades. Initial modeling of autogyro based on the blade element momentum (BEM) approach [1] traces back to Glauert [2] where the author considered constant pitch of the rotor blade. Many researchers developed their model [3]–[7] modifying the assumptions of [2]. Among them, work of Wheatley [5] needs to be mentioned particularly for its significance of providing a detailed model where the author introduced a linear variation in pitch and validated the result experimentally using a commercially available autogyro. Readers are suggested to read [8] and [9] to know further about the development of the autogyro over time.

A tethered rotorcraft can be an effective option for harvesting power from an airborne wind energy (AWE) device at high altitude [10]. The effect of regenerative braking on the steady-state behavior of autogyro and their feasibility for high-altitude power generation have been explored in [11]–[14], where the authors develop their model preliminarily based on [5]. In [15], the equilibrium behaviour of a tethered autogyro in steady-state autorotation is demonstrated for both cases of high-altitude power generation and low-altitude surveillance. In the field of surveillance, tethered autogyro can be considered as an energy saving alternative to drones. But unlike drone, there is an inadequacy of study found in literature regarding the attitude control of such systems. Rye [16] investigated longitudinal stability of such system assuming straight massless tether. Houston [17] described control charactestics of an autogyro based on the analysis test data recorded during flight trials. In [18], altitude and pitch control are presented using a PID controller for vehicular towed autogyro where tether is modeled as massless rod.

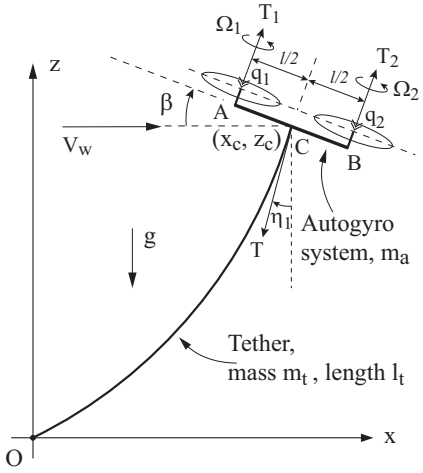

Fig. 1. View of the tethered autogyro in 2-D with two rotors. The system's pitch angle is represented by β.

In this paper, we investigate the dynamic behaviour and equilibrium nature of a multi-rotor autogyro tethered to ground. The dynamic model coupled with a static catenary model incorporating tether mass generates complex dynamic equations which are difficult to solve analytically. Hence, as a starting research study, a 2D case is considered to reduce some of the complexities of the equations, restricting the motion in X-Z plane. The nature of autorotative equilibria are explored. We propose and evaluate the performance of an altitude controller that only uses braking toque as control input for pitch modulation. Simulation results showing the performance of control are presented in VI. Indeed, the dynamical analysis of the proposed quadcopter-based autogyro is only complete when the entire 3D dynamics is considered. The reason for reducing the system to 2D for this study is to

* This work was supported by National Science Foundation grant #1762986.

[1]Tasnia Noboni is a PhD student of Mechanical and Aerospace Engineering at University of Central Florida, Orlando, FL 32816. tasnia.noboni@knights.ucf.edu

[2]Jonathan McConnell is a PhD student of Mechanical and Aerospace Engineering at University of Central Florida, Orlando, FL 32816. Jonathan.McConnell@knights.ucf.edu

[3]Tuhin Das is an associate professor of Mechanical and Aerospace Engineering at University of Central Florida, Orlando, FL 32816. Tuhin.Das@ucf.edu

demonstrate a feasibility of altitude and pitch control using differential braking only. The exclusive use of braking for control is novel in such rotorcrafts and the goal of this paper is to demonstrate its viability within a contained (i.e., 2D) framework as an initial study. Our future work will cover the full 3D dynamics.

II. SYSTEM DESCRIPTION

A. Equations of Motion of the Dynamic System

The system studied in this paper has a two-rotor mechanism and is connected to the ground by a tether as shown in Fig.1. The rotors in this system consist of blades that can flap about their root. As a result, a significant amount of the rolling and pitching motions of each rotor, generated by uneven force distributions, are relieved. The dynamic model of the system is developed under the assumption that thrust force in each rotor is always along the rotor axis. For the overall system, the roll and yaw motions are assumed to be already controlled by other two rotors in lateral direction and that there is no wind velocity in that direction. This assumption allows the system to be studied in the X-Z plane. Solving the equation of motion (1)-(3) gives the position x and z and pitch angle β of the autogyro.

$$m_a\ddot{x} = T_1 \sin\beta + T_2 \sin\beta + d_c(V_w - \dot{x}) - T\sin\eta_1 \quad (1)$$

$$m_a\ddot{z} = T_1 \cos\beta + T_2 \cos\beta - d_c\dot{z} - T\cos\eta_1 - m_a g \quad (2)$$

where, d_c is the damping coefficient. Rotor thrust forces T_1, T_2 and tether tension T comes from aerodynamic model explained in II-B and catenary model described in III respectively.

$$I_c\ddot{\beta} = \frac{l}{2}(T_1 - T_2) \quad (3)$$

where, I_c is the moment of inertia of the frame about its center point C in Fig.1. The system is arranged in such a way that the difference in two thrust forces T_1, T_2 in rotors A and B can cause pitch angle β to change when braking torque q_1 in (4) or q_2 in (5) is applied.

$$I_r\dot{\Omega}_1 = Q_A + q_1 \quad (4)$$

$$I_r\dot{\Omega}_2 = Q_B + q_2 \quad (5)$$

where, I_r is the moment of inertia of each rotor about its rotational axis, R is the radius of the blade, Q_A, Q_B are the aerodynamic torque of rotor A and B respectively. The braking torque causes change in rotational velocities Ω_1 and Ω_2 of each rotor about its respective shaft which is crucial to the aerodynamic properties of the system described in II-B. It subsequently leads to the change in the thrust forces of the system. Thus, with the help of restoring effect from of the tether tension T, position of the system can be changed by the difference in T_1 and T_2.

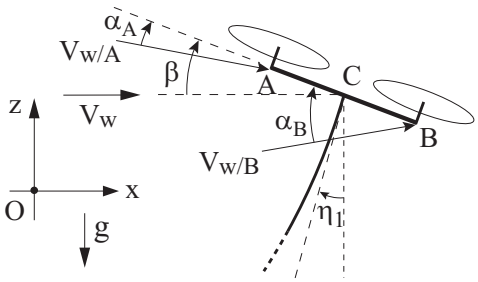

Fig. 2. Setup for calculation of relative velocity and angles of incidence.

B. Aerodynamic Analysis

The aerodynamic model of a tethered autogyro considered in this study is primarily adopted from [15] where work of Wheatley, [5], is taken as a foundation model to study steady autorotation of a tethered autogyro. Since, this paper focuses on the dynamic behaviour, the aerodynamic equations of [5] are rearranged and solved in a more causal manner suitable for capturing the transients. The arrangement of the system, illustrated in Fig.2, causes the rotors to experience relative wind velocity at angle α_A and α_B respectively.

$$\begin{aligned}\vec{V}_{w/A} &= \Big(V_w - \dot{x} - \frac{l}{2}\dot{\beta}\sin\beta\Big)\hat{i} - \Big(\dot{z} + \frac{l}{2}\dot{\beta}\cos\beta\Big)\hat{k} \\ \vec{V}_{w/B} &= \Big(V_w - \dot{x} + \frac{l}{2}\dot{\beta}\sin\beta\Big)\hat{i} - \Big(\dot{z} - \frac{l}{2}\dot{\beta}\cos\beta\Big)\hat{k}\end{aligned} \quad (6)$$

V_w and initial states are provided to (6) to calculate $V_{w/A}$ and $V_{w/B}$. Angle of incidence α_A and α_B are calculated using (7).

$$\begin{aligned}\alpha_A &= \beta - \arctan\frac{\dot{z} + \frac{l}{2}\dot{\beta}\cos\beta}{V_w - \dot{x} - \frac{l}{2}\dot{\beta}\sin\beta} \\ \alpha_B &= \beta - \arctan\frac{\dot{z} - \frac{l}{2}\dot{\beta}\cos\beta}{V_w - \dot{x} + \frac{l}{2}\dot{\beta}\sin\beta}\end{aligned} \quad (7)$$

The equations in (6) and (7) can be derived using kinematic analysis. The aerodynamic model in [15] utilizes two dimensionless ratios μ and λ for each rotor. Tip speed ratio, μ, shown in (8), is the ratio of the wind velocity parallel to the rotor disc to the tip speed of the rotor blade.

$$\mu_A = \frac{V_{w/A}\cos\alpha_A}{\Omega_1 R}, \quad \mu_B = \frac{V_{w/B}\cos\alpha_B}{\Omega_2 R} \quad (8)$$

The inflow ratio, λ, is the ratio of total wind velocity perpendicular to the rotor disc to the tip speed of the rotor blade. The rolling torque of the rotor is balanced by flapping motion of the hinged rotor blade at the base. The flapping angle of the blade is approximated by a periodic function dependent on its angular position, as a truncated Fourier series containing five coefficients [5]. These Fourier coefficients are expressed as functions of λ and μ in [5] and can be re-written as a matrix equation (9).

$$\begin{bmatrix} 1 & 0 & 0 & 0 & v_{15} \\ 0 & 1 & 0 & 0 & v_{25} \\ v_{31} & 0 & 1 & v_{34} & 0 \\ 0 & v_{42} & 0 & 3 & v_{45} \\ v_{51} & 0 & v_{53} & v_{54} & 3 \end{bmatrix} \begin{bmatrix} a_0 \\ a_1 \\ b_1 \\ a_2 \\ b_2 \end{bmatrix} = \begin{bmatrix} A_0 \\ A_1 \\ 0 \\ A_3 \\ 0 \end{bmatrix} \lambda + \begin{bmatrix} C_0 \\ C_1 \\ 0 \\ C_3 \\ 0 \end{bmatrix} \quad (9)$$

where,

$$v_{15} = -\frac{1}{16}\gamma\mu^2 B^2, v_{25} = \frac{2\mu B^3}{3(B^4 - \frac{1}{2}\mu^2 B^2)},$$
$$v_{31} = \frac{-4\mu B}{B^2 + \frac{1}{2}\mu^2}\Big(\frac{1}{3} + \frac{0.035\mu^3}{B^3}\Big),$$
$$v_{34} = \frac{-4\mu B}{6(B^2 + \frac{1}{2}\mu^2)}, v_{42} = -\frac{1}{6}\gamma\mu B^3, v_{45} = -\frac{1}{4}\gamma B^4,$$
$$v_{51} = \frac{1}{8}\gamma\mu^2\Big(B^2 - \frac{\mu^2}{6}\Big), v_{53} = -\frac{1}{6}\gamma\mu B^3, v_{54} = \frac{1}{4}\gamma B^4,$$
$$A_0 = \frac{1}{2}\gamma\Big(\frac{1}{3}B^3 + 0.080\mu^3\Big), A_1 = \frac{\mu(4B^2 - \mu^2)}{2(B^4 - \frac{1}{2}\mu^2 B^2)}$$
$$A_3 = \frac{-0.053}{2}\gamma\mu^3$$
$$C_0 = \frac{1}{2}\gamma\Big\{\frac{\theta_0}{4}\Big(B^4 + \mu^2 B^2 - \frac{1}{8}\mu^4\Big) + \frac{\theta_1}{5}\Big(B^5 + \frac{5}{6}\mu^2 B^3\Big)\Big\} - \frac{M_w}{I_1\Omega^2},$$
$$C_1 = \frac{2\mu}{B^4 - \frac{1}{2}\mu^2 B^2}\Big(\frac{4}{3}\theta_0 B^3 + 0.106\theta_0\mu^3 + \theta_1 B^4\Big)$$
$$C_3 = -\frac{1}{2}\gamma\mu^2\Big\{\frac{\theta_0}{4}\Big(B^2 - \frac{1}{8}\mu^2\Big) + \frac{1}{6}\theta_1 B^3\Big\}$$

Equation (10) can be derived from (9) and solved for 5x1 coefficient matrix $\boldsymbol{\rho_c}$ if λ is known.

$$\boldsymbol{\rho_c} = \boldsymbol{v^{-1}A}\lambda + \boldsymbol{v^{-1}C} \tag{10}$$

a_1 and b_2 from (9) can also be expressed as linear functions of λ shown in (11) and (12).

$$a_1 = m_0\lambda + m_1 \tag{11}$$

$$b_2 = s_0\lambda + s_1 \tag{12}$$

where, $m_0 = A_1$, $m_1 = -v_{25}b_2 + C_1$, $s_0 = 0$, and $s_1 = \frac{-1}{3} - 1(v_{51}a_0 + v_{53}b_1 + v_{54}a_2)$. Equation (11) and (12) help to simplify the calculation of coefficient of rotor thrust C_t. The relation of C_t and λ given in [5], can be rearranged as (13).

$$C_t = p_0 + p_1\lambda + p_2 b_2 + p_3 a_1 \tag{13}$$

where,

$$p_0 = \frac{1}{2}\sigma a\Big\{\theta_0\Big(\frac{1}{3}B^3 + \frac{1}{2}\mu^2 B - \frac{4}{9\pi}\mu^3\Big) + \theta_1\Big(\frac{1}{4}B^4 + \frac{1}{4}\mu^2 B^2 - \frac{1}{32}\mu^4\Big)\Big\},$$
$$p_1 = \frac{1}{4}\sigma a\Big(B^2 + \frac{1}{2}\mu^2\Big), p_2 = \frac{1}{8}\sigma a\mu^2 B,$$
$$p_3 = \frac{1}{16}\sigma a\mu^3$$

Substituting (11) and (12) into (13), we get (14) which expresses C_t as a linear function of λ.

$$\begin{aligned} C_t &= (p_1 + p_2 s_0 + p_3 m_0)\lambda + (p_0 + p_2 s_1 + p_3 m_1) \\ &= c_0\lambda + c_1 \end{aligned} \tag{14}$$

Thus equation (14), a simplified version of (13), is only a function of variable λ if Fourier coefficients are already known by solving (10). The relation among variables α, C_t and λ from [5], given in (15), can be re-written as (16) after replacing C_t with the expression established in (14). Equation (18) provides Q_a and Q_b about each rotor.

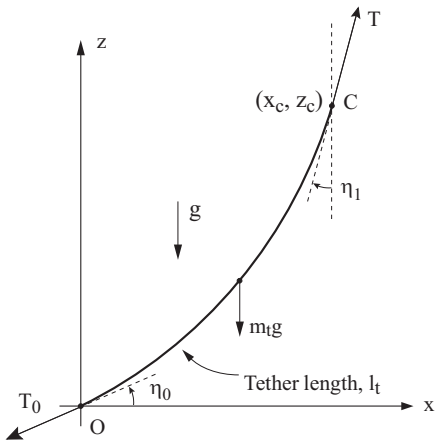

Fig. 3. Static forces on a catenary tether

$$\tan\alpha = \frac{\lambda}{\mu} + \frac{\frac{1}{2}C_t}{\mu(\lambda^2 + \mu^2)^{\frac{1}{2}}} \tag{15}$$

$$\tan\alpha = \frac{\lambda}{\mu} + \frac{\frac{1}{2}c_0\lambda + c_1}{\mu(\lambda^2 + \mu^2)^{\frac{1}{2}}} \tag{16}$$

Equation (10) and (16) are coupled and can be solved only by simultaneous numerical approach. The following numerical process is employed to determine λ and a_0, a_1, b_1, a_2, b_2:

1) A good initial guess of λ is provided to (10) to calculate $\boldsymbol{\rho_c}$ which provides c_0, c_1.
2) λ is approximated using (16).
3) If convergence criteria is not met, guess for λ is adjusted towards the calculated value of λ.
4) Steps 1-3 are repeated until desired convergence is achieved for λ. The threshold value for absolute change in λ is chosen to be 10^{-6}.
5) With converged value of λ, final Fourier coefficients are calculated using (10) at that instant.

This numerical process is implemented for both rotors separately and λ_a, λ_b, $\boldsymbol{\rho_{cA}}$, $\boldsymbol{\rho_{cB}}$ are evaluated. Thrust coefficient, C_{t_1} and C_{t_2}, are calculated with (15) to calculate the thrust force in each rotor using

$$T_1 = \rho\Omega_1^2\pi R^4 C_{t_1}, \quad T_2 = \rho\Omega_2^2\pi R^4 C_{t_2} \tag{17}$$

Equation (17) is used to calculate thrust forces in both rotors. The aerodynamic torque Q about the rotor is zero for steady-state autorotation. For dynamic modeling, Q must be calculated with (18) adopted from [5].

$$\begin{aligned} Q = \frac{1}{2}b\rho c\Omega^2 R^4 a\Big\{&\lambda^2\Big(\frac{1}{2}B^2 - \frac{1}{4}\mu^2\Big) + \lambda\Big(\frac{1}{3}\theta_0 B^3 + \frac{2}{9\pi}\mu^3\theta_0 + \frac{1}{4}\theta_1 B^4 + \frac{1}{32}\mu^4\theta_1\Big) + \mu\lambda a_1\Big(\frac{1}{2}B^2 - \frac{3}{8}\mu^2\Big) \\ &+ a_0^2\Big(\frac{1}{4}\mu^2 B^2 - \frac{1}{16}\mu^4\Big) - \frac{1}{3}\mu a_0 b_1 B^3 + a_1^2\Big(\frac{1}{8}B^4 + \frac{3}{16}\mu^2 B^2\Big) + b_1^2\Big(\frac{1}{8}B^4 + \frac{1}{16}\mu^2 B^2\Big) - a_2\Big(\frac{1}{4}\mu^2 a_0 B^2 \\ &+ \frac{1}{6}\mu b_1 B^3\Big) + \frac{1}{2}a_2^2 B^4 + b_2\Big(\frac{1}{8}\mu^2\theta_0 B^2 + \frac{1}{12}\mu^2\theta_1 B^3 + \frac{1}{6}\mu a_1 B^3\Big) + \frac{1}{2}b_2^2 B^4 - \frac{\delta}{4a}\Big(1 + \mu^2 - \frac{1}{8}\mu^4\Big)\Big\} \end{aligned} \tag{18}$$

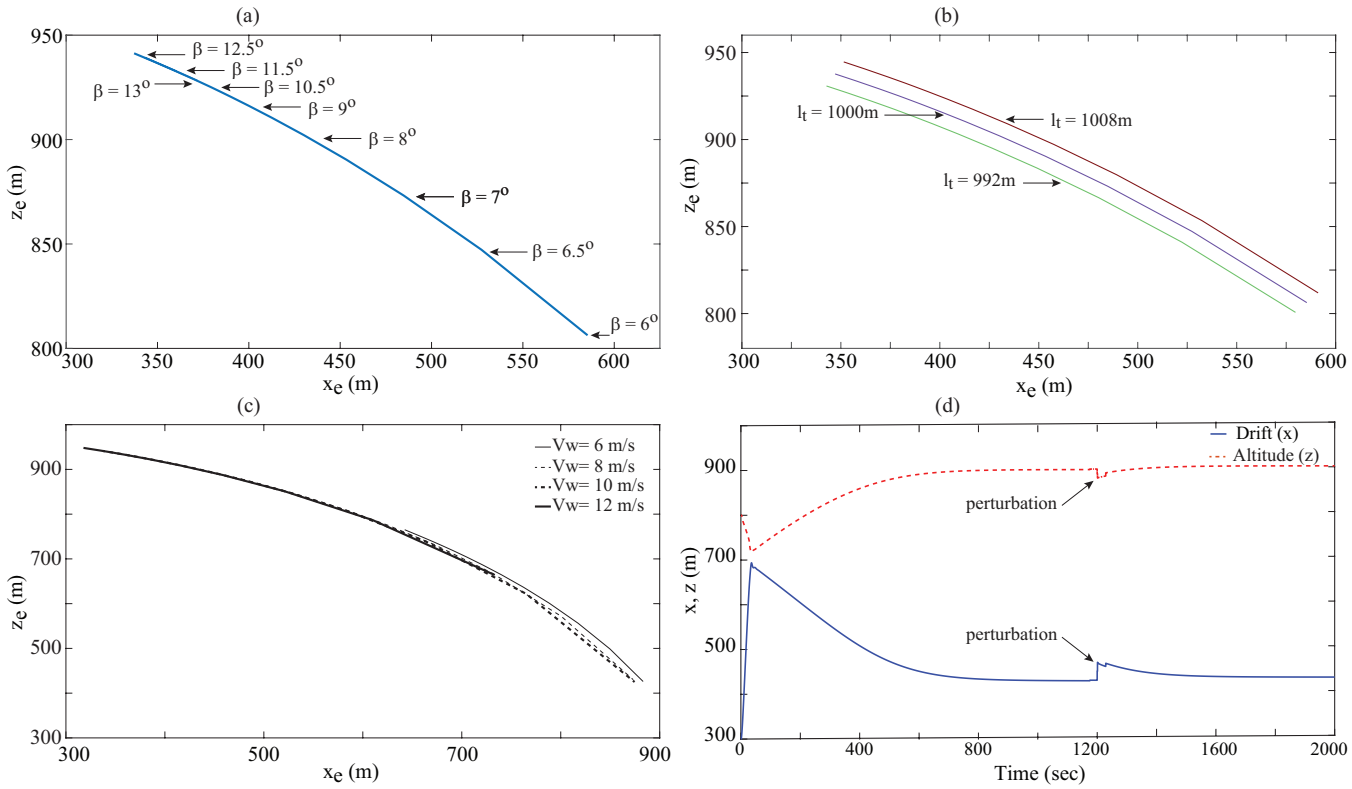

Fig. 4. Characteristics of equilibria: (a) Equilibria at $V_w = 10$m/s and $l_t = 1000$m; (b) Equilibria for varying l_t and at $V_w = 10$m/s for $\beta = 6° - 12°$; (c) Equilibria for varying V_w; (d) Transient behavior of system under perturbation, for $V_w = 10$m/s and $l_t = 1000$m

III. CATENARY

The restoring force in the multi-rotor autogyro system is provided by the tether tension T. To evaluate the tension, a tether profile is approximated using static catenary model adopted from [19] where (19)-(20) define the tether shape.

$$z = \zeta \left[\cosh\left(\frac{x-q}{\zeta}\right) - \cosh\left(\frac{q}{\zeta}\right) \right] \tag{19}$$

$$l_t = \zeta \left[\sinh\left(\frac{x-q}{\zeta}\right) + \sinh\left(\frac{q}{\zeta}\right) \right], \tag{20}$$

where, l_t is length of tether, q and ζ are parameters of the catenary depending on the position and tether length. Equation (19) and (20) together can be manipulated to take the form of (21) and (22).

$$\cosh\left(\frac{x}{\zeta}\right) = 1 + \frac{1}{2\,\zeta^2}\left(l_t^2 - z^2\right) \tag{21}$$

$$q = \frac{x}{2} - \left\{ \zeta \operatorname{arctanh}\left(\frac{z}{l_t}\right) \right\} \tag{22}$$

Equation (21) is numerically solved to determine ζ. With known ζ, q can be easily calculated from (22) for a known l_t and known end point (x, z) of the tether which in this case is the center point of the frame. q and ζ are used to calculate angle η_0 and η_1 using (23)-(24) from [19].

$$\eta_0 = \arctan\left\{ -\sinh\left(\frac{q}{\zeta}\right) \right\} \tag{23}$$

$$\eta_1 = \frac{\pi}{2} - \arctan\left(\frac{l_t}{\zeta} + \tan\eta_0\right) \tag{24}$$

Fig.3 shows the setup for static analysis of the catenary. η_0 and η_1 possess two constraints for the system to be valid and they are- (i) $\eta_0 + \eta_1 < 90°$ and (ii) $\eta_0 > 0°$. Static force balance equations at the two end points of the catenary is given in (25).

$$\begin{aligned} T\sin\eta_1 - T_0\cos\eta_0 &= 0 \\ T\cos\eta_1 - T_0\sin\eta_0 - m_t g &= 0 \end{aligned}, \tag{25}$$

where, m_t is the mass of the tether. We can eliminate T_0 from (25) and determine T knowing η_0 and η_1 from (23) and (24) respectively. The expression for T is given in (26),

$$T = \frac{\sigma_t l_t g \cos\eta_0}{\cos(\eta_0 + \eta_1)}, \tag{26}$$

where σ_t is the mass per unit length of the tether.

IV. CHARACTERISTICS OF EQUILIBRIA

With suitable parameter values from [15] and initial guesses for states, the equations of motion in (1)-(5) can be solved and simulated following the steps described in Section II. The solution converges to equilibrium without any external control input, yielding an equilibrium space similar to that in [15]. The convergence indicates stability of the equilibria. Figure 4(a) shows the variation of the equilibrium points with varying incidence angle β for fixed wind speed V_w and fixed tether length l_t. With increasing β, the equilibrium altitude increases up to a certain β (12.5° in this case), and reduces thereafter. The reduction is attributed

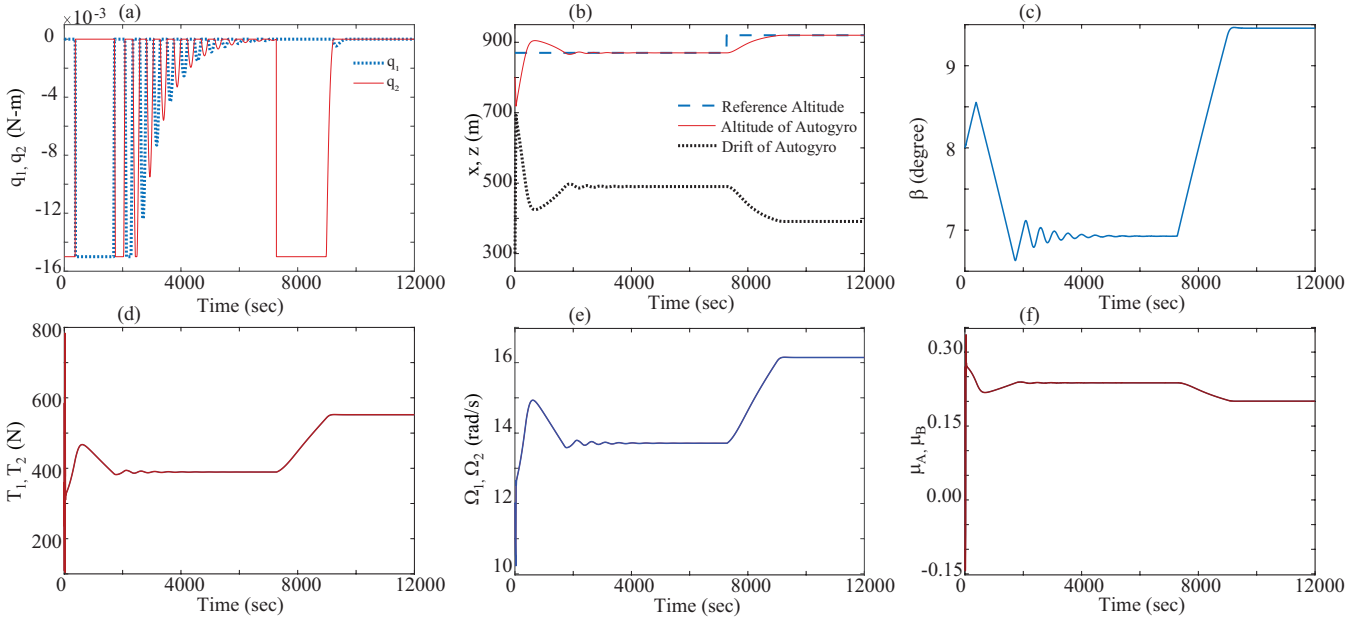

Fig. 5. Altitude control in uniform wind speed: (a) Applied braking torques as control input; (b) Change in altitude and drift with time, reference altitude set at 870m and 920m; (c) Pitching angle of the system; (d) Thrust forces T_1 and T_2; (e) Rotational speeds Ω_1 and Ω_2; (f) Tip-speed ratios μ_A and μ_B in the presence of control action

to the aerodynamic forces becoming dominated by drag. The drag-dominated region corresponds to low values of μ, $\mu \leq 0.15$, where the momentum theory becomes less reliable. For the purposes of control development, this region is avoided.

The equilibrium points also depend on V_w and l_t. Figure 4(b) shows that for $V_w = 10$m/s, the envelope of equilibria shifts up with increasing l_t. On the other hand, the dependency of equilibrium points on V_w at a fixed $l_t = 1000$m shown in Fig.4(c) suggests that as expected, higher feasible elevations happen at higher values of V_w. Figure 4(c) also indicates a narrow operating range at low V_w, which gets wider with increasing wind speed. It is evident that without any control, the system attains equilibrium for uniform V_w, fixed l_t and fixed β. This is evident from Fig.4(d). Here, at $t = 1200$s the position is perturbed from its equilibrium position, (x_e, z_e). We observe that the equilibrium is restored subsequently. This indicates an internally stable equilibrium of the 2D autogyro system, at least for small perturbations. The corresponding stability analysis is an area of our ongoing research.

V. ALTITUDE CONTROL VIA DIFFERENTIAL ROTOR BRAKING

An autorotating rotor is unpowered and uses the ambient wind energy to generate the necessary thrust force. In the 2-D multi-rotor system considered in this work, we demonstrate that differential braking of the individual autorotating rotors can be used for altering its pitch angle β and thereby achieve altitude control. From (4) and (5), it is evident that braking torques q_1 and q_2 will tend to reduce the corresponding angular velocities Ω_1 and Ω_2. Equations (17) and (3) show that differential braking will cause the thrusts T_1 and T_2 to differ and thereby cause β to change. Figure 4(a) shows that the change in β, produced by differential braking, will lead to altitude change. We next present a controller that achieves this goal.

A proportional feedback control algorithm is employed in this study to enable the autogyro to reach to a desired altitude in the presence of both uniform and variable wind field. In Section V-A, it is shown that the proportional control leads to an integral effect in the dynamics of $(z - zd)$. This enables the error $(z - zd)$ to go to zero. The algorithm requires one control input at each rotor, namely the braking torque q_1 and q_2. The control law, given in (27), generates braking a torque on either rotor A or B. The braking torque q_1, when applied on rotor A, momentarily decreases the thrust T_1 leading to decrease in β, and eventually altitude is decreased. In the same way, braking torque q_2 in rotor B increases β, thereby increasing altitude.

$$q_1 = \begin{cases} K_p(z_d - z) & \text{for} \quad z > z_d \\ 0 & \text{for} \quad z \leq z_d \end{cases}$$
$$q_2 = \begin{cases} 0 & \text{for} \quad z \geq z_d \\ -K_p(z_d - z) & \text{for} \quad z < z_d \end{cases} \tag{27}$$

Here, K_p is the controller gain and z_d is the desired altitude. The control input is allowed to take a value between 0 and an upper limit depending on the error signal. Small braking torques are sufficient to cause gradual changes in β. Drastic change in β are problematic and can induce instabilities.

A. Approximate Closed-Loop Dynamics

We next derive an approximate closed-loop dynamics, which helps explain why the control law of (27) is effective in altitude control. Consider the dynamics of the variable

$\tilde{z} = (z - z_d)$. Referring to (2),

$$\begin{aligned}(T_1 + T_2)\cos\beta &= (T_1 - T_2)\cos\beta + 2T_2\cos\beta \\ &= 2\frac{I_c}{l}\ddot{\beta} + 2T_2\cos\beta\end{aligned} \tag{28}$$

Simulations indicate that the slow dynamics of β can be approximated by,

$$\dot{\beta} = k_1(q_1 - q_2), \tag{29}$$

and from (27),

$$(q_1 - q_2) = K_p(z_d - z) = -K_p\tilde{z}. \tag{30}$$

Thus, for small perturbations around an equilibrium $z = z_d$,

$$\begin{aligned}(T_1+T_2)\cos\beta = (2T_2\cos\beta)\,|_{eq} \\ - 2\frac{I_c}{l}k_1K_p\dot{\tilde{z}} - \left[\frac{d}{d\beta}(2T_2\cos\beta)\right]_{eq}k_1K_p\int_0^t\tilde{z}dt\end{aligned} \tag{31}$$

The time integral appears in (31) due to the fact that from (29) and (30), $d\beta = -K_p\int_0^t\tilde{z}dt$. From Section III, the catenary tension forces are position dependent only and not velocity dependent. Hence, the tether tension force in (2) can be expressed about the equilibrium as

$$T\cos\eta_1 = (T\cos\eta_1)\,|_{eq} - k_{zz}\tilde{z} - k_{zx}\tilde{x} \tag{32}$$

where $\tilde{x}$ is the small deviation of the x-coordinate of the autogyro from its equilibrium. Together, an approximate dynamic equation of the system in the $\tilde{z}$ coordinate would have the structure

$$\begin{aligned}m_a\ddot{\tilde{z}} = -\left(d_c + 2\frac{I_c}{l}k_1K_p\right)\dot{\tilde{z}} - k_{zz}\tilde{z} - k_{zx}\tilde{x} \\ - \left[\frac{d}{d\beta}(2T_2\cos\beta)\right]_{eq}k_1K_p\int_0^t\tilde{z}dt\end{aligned} \tag{33}$$

While the above dynamic equation is not complete and other terms such as the aerodynamic drag forces must be included and (33) must be considered in conjunction with the corresponding dynamic equation of $\tilde{x}$, it gives an idea of the structure. Equation (33) shows the damping and restoring forces and their sources. It also indicates that robust convergence to z_d may be achieved due to the effective integral action provided by the controller. Further study will investigate the stability characteristics of the equilibrium under the closed loop control of (27) which is an area of ongoing work.

VI. SIMULATION RESULT

A. Uniform Wind Field

In a uniform wind speed of 10m/s and fixed tether length of 1000m, the proposed controller with $K_p = 0.01$ controls the system's altitude within the operating region. The simulation result in Fig.5 shows that the autogyro settles at the desired altitudes of 870m and 920m without any steady-state error, which may be attributed to the integral action provided by the proposed controller. The applied braking torques in each rotor are allowed to take a value between 0 and -0.015Nm. This leads to a slow control action but demonstrates the viability of the controller. Fig.5(a) confirms that the braking torques are mutually exclusive as evident from (27). The oscillatory behavior in β, as evidenced in Fig.5(c), may be reduced by better tuning of the controller or by addition of a derivative action. Finally, we note that the thrusts T_1 and T_2 differ from each other during transients. In Fig.5(d) these differences are indiscernible but can be seen when zoomed in to the transient regions. The same is true for Ω_1 and Ω_2 in Fig.5(e) and μ_A and μ_B in Fig.5(f).

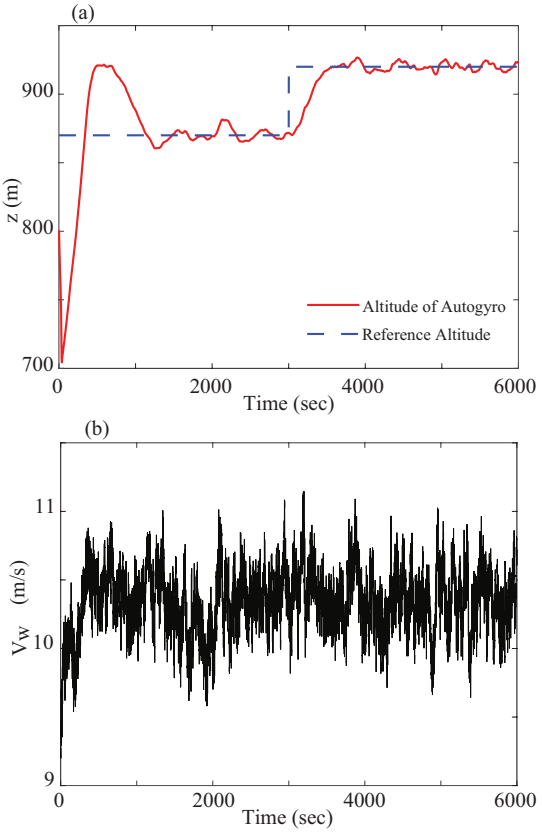

Fig. 6. Altitude control in the presence of variable wind speed: (a) reference set at 870m and 920m; (b) variable wind profile generated by TurbSim

B. Variable Wind Field

In this section, performance of the controller in the presence of variable wind profile, a practical scenario, is explored. Figure 6(a) illustrates that the autogyro goes to the desired altitude z_d within the operating region with an acceptable diversion from the set point when the control torques are applied. The variable wind speed is generated by TurbSim and illustrated in Fig.6(b). The range of control input as braking torque is selected to be between 0 and -0.05Nm with $K_p = 0.02$ which is higher than uniform wind speed case. This is owing to the greater control effort required for variable wind speeds, which is expected. From Figs. 5(b) and 5(c), it is evident that change in altitude is very sensitive to changes in β. Hence Kp values were chosen to be small to regulate changes in β through q_1 and q_2.

VII. CONCLUSIONS

This study develops a dynamic model of a tethered autogyro extending the system described in [15], combined with a catenary mechanism to explore the dynamic behaviour. The proposed model is simulated numerically to study the correlation of equilibrium space and operating conditions with varying pitch angle, tether length and wind speed. The equilibrium space follows the trend of steady-state conditions in [15]. The model however extends to transient simulations, amenable for control development. A feedback controller providing differential braking of the rotors is used to control the altitude and the results show good agreement in the uniform field. The control law is then applied to the variable wind profile case. As this work is an initial study of control application on the tethred autogyro, we believe control design based on a further improved dynamic model will provide more credibility for practical application. Thus, our future work will be focused areas such as relaxing the assumptions of thrust forces being always along the rotor axes and incorporating tether aerodynamics in greater detail.

NOMENCLATURE WITH PARAMETER VALUES

x, x_e	Autogyro drift & horizontal equilibrium
z, z_e	Autogyro altitude & vertical equilibrium
β	Pitch angle
g	Acceleration due to gravity
d_c	Damping constant $(10Ns/m)$
Ω_1, Ω_2	Angular velocity of rotor A & B
V_w	Wind velocity
$V_{w/A}, V_{w/B}$	Relative wind velocity at rotor A & B
α_A, α_B	Angle of incidence at rotor A & B
μ_A, μ_B	Tip speed ratio of rotor A & B
λ_A, λ_B	inflow ratio of rotor A & B
$a_0, a_1, b_1,$ a_2, b_2	Fourier coefficients
b	Number of blades (4)
l	Length of frame $(8.13m)$
R	Blade radius $(3.048m)$
m_a	Total mass of the autogyro $(35.94Kg)$ including frame
I	Blade moment of inertia about flapping hinge $(7.884kgm^2)$
I_r	Rotor moment of inertia $(73.72kgm^2)$
I_c	Moment of inertia of the system about center point $(547.61kgm^2)$
c	Blade chord $(0.24384m)$
θ_0	Blade pitch angle at hub $(0.0384rad)$
θ_1	Blade pitch slope $(4.9448^{-03}rad/m)$
B	Blade radius fractionless tip losses(0.96)
a	Slope of lift curve (5.85)
δ	Average drag coefficient (0.012)
ρ	Density of air $(1.225kgm^{-3})$
σ	Blade disc solidity (0.1019)
γ	Non-dimensional mass constant (19.1298)
M_W	Flapping moment from blade weight $(37.9625Nm)$
C_{t_1}, C_{t_2}	Rotor thrust coefficient
T_1, T_2	Thrust force in rotor A & B
T_0, T	Tether tension at base and at end
η_0	Tether angle at base with horizontal
η_1	Tether angle at autogyro with vertical
σ_t	Mass per unit length of tether $(0.0148kg/m)$
m_t	Mass of tether
l_t	Length of tether

REFERENCES

[1] A. Gessow and G. C. Myers Jr., *Aerodynamics of the Helicopter*. Macmillan Company, New York, 1952.

[2] H. Glauert, "A general theory of the autogyro," *Presented by the Director of Scientific Research Air Ministry, Reports and Memoranda No. 1111 (Ae. 285)*, 1926.

[3] C. N. H. Lock, "Further development of autogyro theory - part 1," *National Advisory Committee for Aeronautics, Reports and Memoranda No. 1127 (Ae. 299)*, 1927.

[4] C. N. H. Lock, "Further development of autogyro theory - part 2: A general treatment of the flapping motion," *National Advisory Committee for Aeronautics, Reports and Memoranda No. 1127 (Ae. 299)*, 1927.

[5] J. B. Wheatley, "An aerodynamic analysis of the autogiro rotor with a comparison between calculated and experimental results," Tech. Rep., 1935.

[6] A. Gessow and A. D. Crim, "An extension of lifting rotor theory to cover operations at large angles of attack and high inflow conditions," *National Advisory Committee for Aeronautics, Technical Note No. 2665*, 1952.

[7] A. Cuerva, A. Sanz-Andres, J. Mesegeur, and J. L. Espino, "An engineering modification of the blade element momentum equation for vertical descent: An autorotation case study," *Journal of the American Helicopter Society*, vol. 51, no. 4, pp. 349–354, 2006.

[8] B. H. Charnov, *From Autogiro to Gyroplane: The Amazing Survival of an Aviation Technology*. Praeger Publishers, Westport CT, 2003.

[9] J. G. Leishman, *Principles of Helicopter Aerodynamics*. Cambridge University Press, 2000.

[10] B. W. Roberts, D. H. Shepard, K. Caldeira, M. E. Cannon, D. G. Eccles, A. J. Grenier, and J. F. Freidin, "Harnessing high-altitude wind power," *IEEE Transactions on Energy Conversion*, vol. 22, pp. 136–144, 2007.

[11] B. Salih, "An introductory study of the dynamics of autorotation for wind energy harvesting," Master's thesis, University of Central Florida, 2014.

[12] S. Rimkus and T. Das, "An application of the autogyro theory to airborne wind energy extraction," *ASME Dynamic Systems and Control Conference (DSCC), Palo Alto, CA*, October, 2013.

[13] S. Mackertich and T. Das, "A quantitative energy and systems analysis framework for airborne wind energy conversion using autorotation," ser. ACC. Boston, MA: IEEE, 2011, pp. 4996–5001.

[14] S. Mackertich, "Dynamic modeling of autorotation for simultaneous lift and wind energy extraction," Master's thesis, University of Central Florida, 2016.

[15] J. McConnell and T. Das, "Equilibrium behavior of a tethered autogyro: Application in extended flight and power generation," *Journal of Applied Mechanics*, vol. 89, no. 9, p. 091003, 2022.

[16] D. C. Rye, "Longitudinal stability of a hovering, tethered rotorcraft," *Journal of Guidance, Control, and Dynamics*, vol. 8, no. 6, pp. 743–752, 1985. [Online]. Available: https://doi.org/10.2514/3.20050

[17] S. S. Houston, "Identification of autogyro longitudinal stability and control characteristics," *Journal of Guidance, Control, and Dynamics*, vol. 21, no. 3, pp. 391–399, 1998. [Online]. Available: https://doi.org/10.2514/2.4271

[18] Y. Ma, Z. Cai, N. Liu, and Y. Wang, "System composition and longitudinal motion control simulation of vehicular towed autogyro," in *2016 IEEE Chinese Guidance, Navigation and Control Conference (CGNCC)*. IEEE, 2016, pp. 1018–1023.

[19] S. Rimkus, T. Das, and R. Mukherjee, "Stability analysis of a tethered airfoil," *2013 American Control Conference*, pp. 5601–5606, 2013.